High resolution computational unsteady aerodynamic techniques applied to manoeuvring UCAVs

S. A. Morton and R. M. Cummings
Department of Aeronautics
USAF Academy, Colorado
USA

J. R. Forsythe and K. Wurtzler
Cobalt Solutions, LLC
Springboro, Ohio
USA

ABSTRACT

A method of high resolution simulation is proposed for Unmanned Combat Air Vehicles (UCAVs) undergoing manoeuvress at high angle-of-attack or transonic speeds. Motivation for the need to develop such a method is first presented to show payoff in the design cycle, followed by results of using the method on current manned fighter aircraft. Finally, a notional UCAV shape from Boeing military aircraft is presented to show the possibilities of how the method can accurately capture the relevant phenomenon of these difficult flight regimes

1.0 INTRODUCTION

Unmanned air vehicles (UAVs) have shown their value as reconnaissance vehicles, and even tactical weapons, over the past few years. Aircraft such as Predator and Global Hawk are fast becoming essential tools in the day-to-day operations of the US military. While the capability of these aircraft will continue to be improved, a need will develop for the vehicles to be able to perform more complex maneuvres to fulfill Unmanned combat air vehicle (UCAV) missions such as delivering munitions or even air-to-air combat.

UCAVs are poised to take advantage of new technology such as control actuation[1], morphing wings[2], fuel-cell-based propulsion systems[3], MEMS-based control systems[4], and semi-autonomous flight[5] and will be essential to the further development of these vehicles.

Another possible use of UCAVs is super-manoeuverability and agility (or pulling many more *g*'s than current fighters). Although the utility of super-manoeuverability is controversial, a simulation technology for super-manoeuverability is necessary to adequately analyze the usefulness of UCAVs in this area. One category of super-manoeuverability is dynamic lift (also known as dynamic stall) due to fast pitch-up maneuvres.

Dynamic lift utilises the hysteresis effects of aerofoils or wings pitching up at rapid rates to delay the onset of stall. As aerofoils pitch up there is a time lag in the separation of flow over the upper surface, which allows for the attainment of higher angles of attack than during static conditions. In addition, leading-edge vortices form that aid in the development of lift. Several researchers have shown the effects of dynamic lift (or dynamic stall) on aerofoils, both with experimental and numerical studies[6-8]. In fact, excellent review articles on dynamic stall have been written by Ekaterinaris and Platzer[9], as well as Carr[10]. Experimental and numerical studies have also been conducted on wings undergoing dynamic stall – see Refs 11 to 13, for example.

Very little work, however, has been done on studying the dynamic lifting capabilities of full aircraft configurations such as generic UCAVs. This is due in part to the lack of an accurate method of simulating full aircraft at flight Reynolds numbers for these complex maneuvres. A numerical method must be able to accurately capture phenomena such as vortex-vortex, vortex-boundary layer, shock-vortex, and shock-vortex-boundary-layer interactions. The pacing item in simulating these phenomena is turbulence modeling.

Paper No. 2876. Manuscript received 12 February 2004, revised 14 July 2006 accepted 4 May 2007.
This paper is declared a work of the US Government and is not subject to copyright protection in the United States.

https://doi.org/10.1017/S0001924000004656 Published online by Cambridge University Press

Computational fluid dynamics (CFD) has remained limited as a reliable tool for prediction of inherently unsteady flows at flight Reynolds numbers due to the unreliability of turbulence models for separated flows. There are three main categories of approaches for simulation of these unsteady separated flowfields: direct numerical simulation (DNS), large eddy simulation (LES), and Reynolds-average Navier-Stokes simulations (RANS). A DNS approach solves the Navier-Stokes equations without use of an explicit turbulence model, requiring every scale of turbulent motion to be resolved. Since the smallest scales of turbulence (Kolmogorov length scales) decrease in size with Reynolds number, simulations are limited to very low Reynolds numbers, as well as fairly simple geometries due to computer limitations. Using extrapolation of current computational resources, Spalart determined that a DNS of a full aircraft would not be possible until the year 2080[14].

LES solves the Navier-Stokes equations with a sub-grid-scale turbulence model, allowing resolution of the large, energy-containing scales of the turbulent flow and modeling only the small-scale eddies that are not resolved by the grid. LES must capture the turbulent scales in the boundary layer for wall-bounded flows (such as full aircraft) to obtain the proper boundary layer. If the boundary layer is not captured correctly, the flow may separate early in regions of high curvature and not correctly capture the attached nature of the actual boundary layer. Spalart estimates LES of full aircraft will not be possible until the year 2045[14].

RANS methods model the entire spectrum of turbulent motion and are feasible today. While often adequate in steady flows with no regions of reversed flow, or possibly exhibiting shallow separations, it appears inevitable that RANS turbulence models are unable to accurately predict phenomena dominating flows characterised by massive unsteady separations. Unsteady massively separated flows are characterised by geometry-dependent and three dimensional turbulent eddies. These eddies, arguably, are what defeats RANS turbulence models in accurately predicting flow of any complexity.

To overcome the deficiencies of RANS models for predicting massively separated flows, Spalart *et al*[15] proposed Detached-Eddy Simulation (DES) with the objective of developing a numerically feasible and accurate approach combining the most favorable elements of RANS models and LES. The primary advantage of DES is that it can be applied at high Reynolds numbers as can Reynolds-averaged techniques, but also resolves geometry-dependent, unsteady three-dimensional turbulent motions as in LES. DES requires essentially the same computational resources as unsteady RANS simulations with some possible increase in run time from grid refinement in separated flow regions. DES predictions to date have been favorable, forming one of the motivations for using this technique for manoeuvring UCAVs. The goal would be to apply DES to UCAVs to first demonstrate the utility of using UCAVs at high g conditions, determine optimal maneuvre profiles, and to eliminate costly flight tests in these difficult portions of the aircraft envelope. The following sections will outline the method, show results of several full aircraft DES predictions with comparison to experiments or flight tests, and finally demonstrate the method on the generic Boeing 1301 UCAV configuration.

2.0 NUMERICAL METHOD

In this section a brief description of the numerical method is provided. Full details of the computational scheme are presented in Ref. 16. Solutions for all configurations were computed with the Cobalt Navier-Stokes solver developed by Cobalt Solutions, LLC. Cobalt solves the unsteady, three-dimensional, compressible Navier-Stokes equations on a hybrid unstructured grid. The code has several choices of turbulence models, including Spalart Almaras (SA), and Menter's Shear Stress Transport (SST) RANS, as well as DES versions of SA and SST. All simulations were computed on unstructured meshes with prisms in the boundary layer and tetrahedra elsewhere. The computational meshes were generated with the software packages GridTool[17] and VGRIDns[18].

2.1 Turbulence models

For simulation of turbulent flows, the governing equations are suitably averaged (time averaged for RANS or filtered for LES), yielding turbulent stresses that require a model. A Boussinesq approximation is invoked in the momentum equations and the turbulent eddy viscosity (μ_t) is used to relate the stresses to the strain rate. The turbulent heat flux is also modeled using a gradient-transport hypothesis, requiring specification of a turbulent thermal conductivity, k_t. The Reynolds analogy is applied and the turbulent heat flux is modeled using a constant turbulent Prandtl number of 0·9. Using turbulent eddy viscosity and turbulent conductivity, the variable μ is replaced by $(\mu + \mu_t)$ and k is replaced by $(k + k_t)$ in the governing equations.

2.2 Spalart-Allmaras turbulence model

The Spalart-Allmaras[19] one equation model (SA) solves a single partial differential equation for a working variable ν which is related to the turbulent viscosity. The differential equation is derived by 'using empiricism and arguments of dimensional analysis, Galilean invariance and selected dependence on the molecular viscosity'[19]. The model includes a wall destruction term that reduces the turbulent viscosity in the laminar sublayer. The model takes the form;

$$\frac{\mathrm{D}\tilde{\nu}}{\mathrm{D}t} = c_{b1}\tilde{S}\tilde{\nu} - c_{w1}f_w\left[\frac{\tilde{\nu}}{d}\right]^2 + \frac{1}{\sigma}\left[\nabla\cdot\left((\nu+\tilde{\nu})\nabla\tilde{\nu}\right) + c_{b2}\left(\nabla\tilde{\nu}\right)^2\right]. \quad \ldots(1)$$

The turbulent kinematic viscosity is obtained from;

$$_t = \frac{\mu_t}{\rho} = \tilde{\nu}f_{v1}, \quad f_{v1} = \frac{\chi^3}{\chi^3 + c_{v1}^3}, \quad \chi \equiv \frac{\tilde{\nu}}{\nu} \quad \ldots(2)$$

where S is the magnitude of the vorticity given by;

$$S = |\omega| = \left|\nabla\times\left(u\hat{i} + v\hat{j} + w\hat{k}\right)\right|, \quad \ldots(3)$$

and the modified vorticity is;

$$\tilde{S} \equiv S + \frac{\tilde{\nu}}{\kappa^2 d^2}f_{v2}, \qquad f_{v2} = 1 - \frac{\chi}{1+\chi f_{v1}}, \quad \ldots(4)$$

where d is the distance to the closest wall. The wall destruction function f_w is;

$$f_w = g\left[\frac{1+c_{w3}^6}{g^6 + c_{w3}^6}\right]^{\frac{1}{6}}, \quad \ldots(5)$$

and

$$g = r + c_{w2}\left(r^6 - r\right) \qquad r \equiv \frac{\tilde{\nu}}{\tilde{S}\kappa^2 d^2}. \quad \ldots(6)$$

The turbulent viscosity is obtained from the turbulent kinematic viscosity by $\mu_t = \rho\nu_t = \rho\tilde{\nu}f_{v1}$

The model coefficients are,

$$\begin{array}{lll} c_{b1} = 0.1355 & \sigma = 2/3 & c_{b2} = 0.622 \\ \kappa = 0.41 & c_{w1} = c_{b1}/\kappa^2 + (1+c_{b2})/\sigma & c_{w2} = 0.3 \\ c_{w3} = 2 & c_{v1} = 7.1 & \end{array} \quad \ldots(7)$$

https://doi.org/10.1017/S0001924000004656 Published online by Cambridge University Press

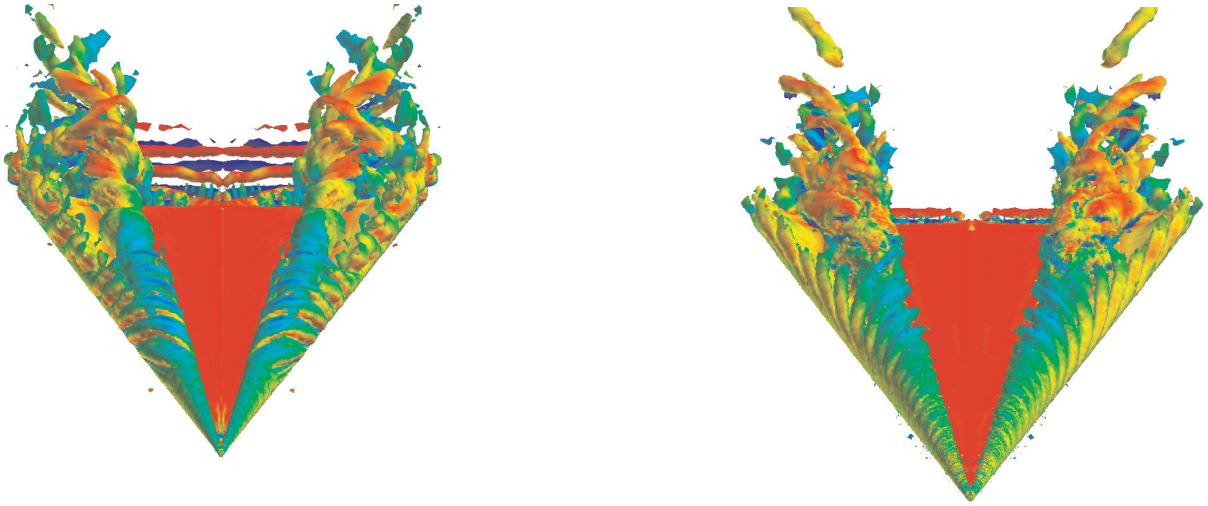


Figure 1. Flow visualisation of a 70° delta wing at 27° angle-of-attack. Iso-surfaces of vorticity. part (a) used 10·5 million and part (b) uses 3·5 million cells.

2.3 Detached-eddy simulation

The detached-eddy simulation method was proposed by Spalart *et al*[15] and was originally based on the Spalart-Allmaras one equation RANS turbulence model (detailed above with a more detailed presentation in Ref. 19). The wall destruction term presented above is proportional to $(\tilde{\nu}/d)^2$, where d is the distance to the wall. When this term is balanced with the production term, the eddy viscosity becomes proportional to $\tilde{S}d^2$ where $\tilde{S}$ is the local strain rate. The Smagorinski LES model varies its sub-grid scale (SGS) turbulent viscosity with the local strain rate, and the grid spacing: $\nu_{SGS} \propto \hat{S}\Delta^2$, where $\Delta = \max(\Delta x,\Delta y,\Delta z)$. If d is replaced with Δ in the wall destruction term, the S-A model will act as a Smagorinski LES model.

To exhibit both RANS and LES behavior, d in the SA model is replaced by;

$$\tilde{d} = \min\left(d, C_{DES}\Delta\right) \quad \ldots (8)$$

When $d<<\Delta$, the model acts in a RANS mode and when $d>>\Delta$ the model acts in a Smagorinski LES mode. Therefore the model switches into LES mode when the grid is locally refined.

DES was implemented in an unstructured grid method by Forsythe *et al*[20]. They used a DES constant of 0·65, consistent with the structured grid implementation of Shur *et al* [21] when the grid spacing was taken to be the longest distance between the cell center and all of the neighbouring cell centres.

A Newton sub-iteration method is used in the solution of the system of equations to improve time accuracy of the point-implicit method and approximate Jacobians. In the calculations presented below, a typical number of three Newton sub-iterations is used for all time-accurate cases.

2.4 Grid generation

Spalart[22] described the process of grid design and assessment for DES, defining important regions of the solution and offering guidelines for grid densities within each region. The 'Young-Person's Guide'[22] (YPG) forms a basis for interpretation of many of the results presented below. One of the traditional motivations for using unstructured grids has been the ability to rapidly create grids around complex geometries. There are other positive attributes of unstructured grids that are relevant to DES. Most notably, it is possible to concentrate points in the region of interest (i.e. the vortex core or aft of breakdown) and rapidly coarsen the grid away from these areas. This region of interest was termed the 'focus region' in the YPG. Another advantage exploited in the present study is the isotropic cells generated in the LES region by most unstructured grid generation packages. The YPG reference describes the desirability of having nearly-isotropic grid cells in the focus region in which unsteady, time-dependent, features are resolved.

Morton *et al*[22] applied the YPG guidelines to three massively separated flows of interest: forebody in a cross-flow, flow over a delta wing at 27° angle-of-attack, and the flow over an F-15E at 65° angle-of-attack. In the latter two cases an extensive grid sensitivity study was performed by systematically varying the grid by a scale parameter allowing a very consistent analysis of grid effects when using the DES method of computing massively separated flows. DES of the F-15E provided an impressive lift, drag, and moment coefficient match of 5% to the Boeing flight test data at 65° angle-of-attack. A more detailed look at the simulations can be found in Ref. 24 and Ref. 25.

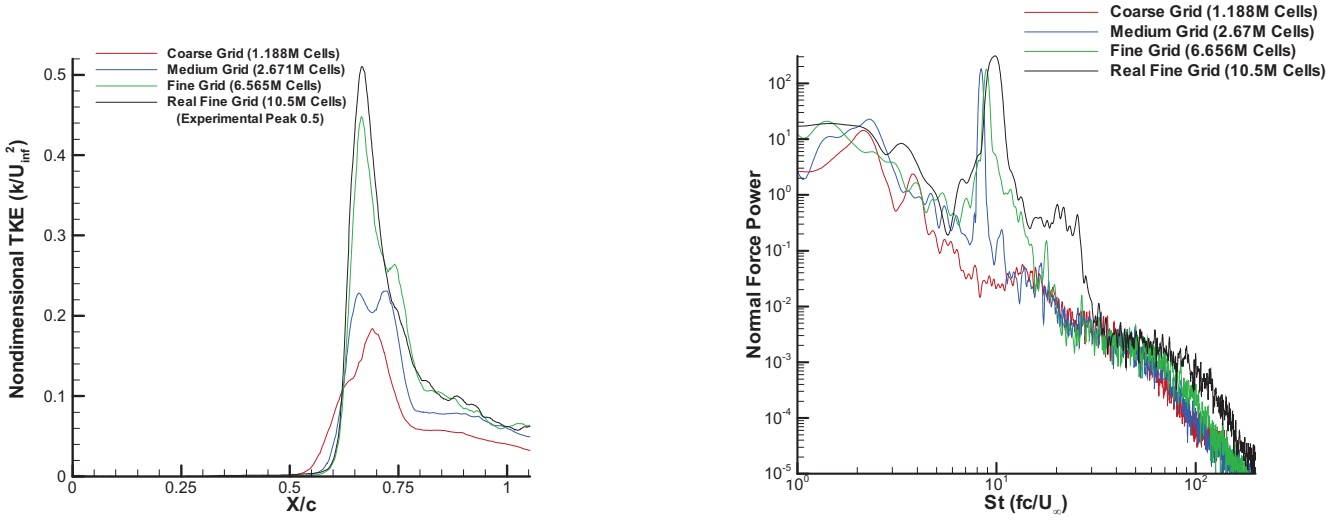
Another important grid technology that is particularly well suited for DES is adaptive-mesh refinement. Pirzadeh[26] presented a method based on a tetrahedral unstructured grid technology developed at NASA Langley Research Center with application to two configurations with vortex dominated flowfields. The large improvement of the adapted solutions in capturing vortex flow structures over the conventional un-adapted results was demonstrated by comparisons with wind-tunnel data. Pirzadeh showed the numerical prediction of these vortical flows was highly sensitive to the local grid resolution and he also stated that grid adaptation is essential to the application of CFD to these complicated flowfields. His most successful computations were performed using an inviscid method due to the inadequacies of standard turbulence models in computing these complicated flow fields. For the current work a mean flow solution on a baseline grid is used to create an adaptively-refined mesh and the new grid is used with DES to compute the unsteady flow field.

2.5 Summary of the proposed method

The proposed method for simulating UCAVs undergoing rapid manoeuvring is as follows:

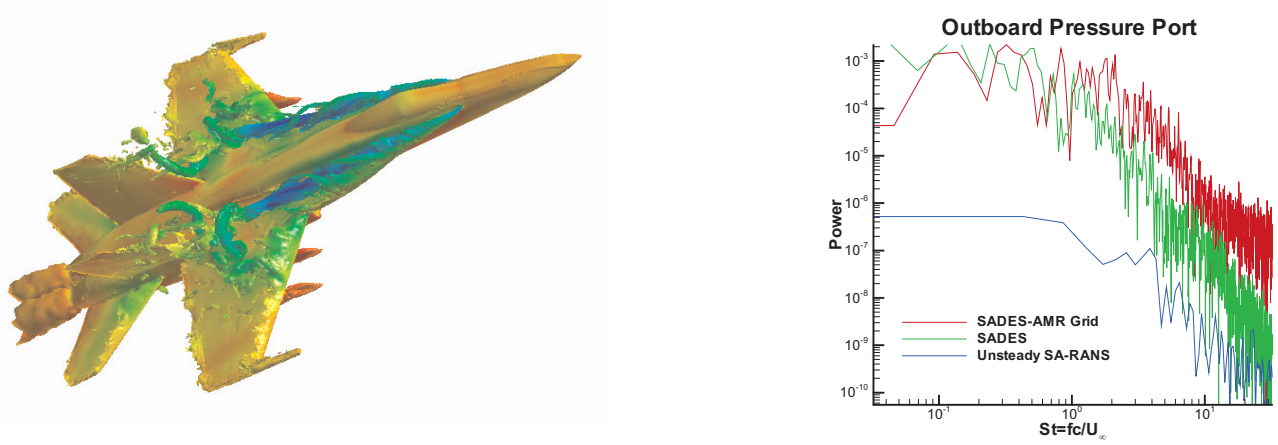
1. Use a time-accurate unstructured grid solver to allow rapid turn around of grids on complex configurations – must have at least

https://doi.org/10.1017/S0001924000004656 Published online by Cambridge University Press



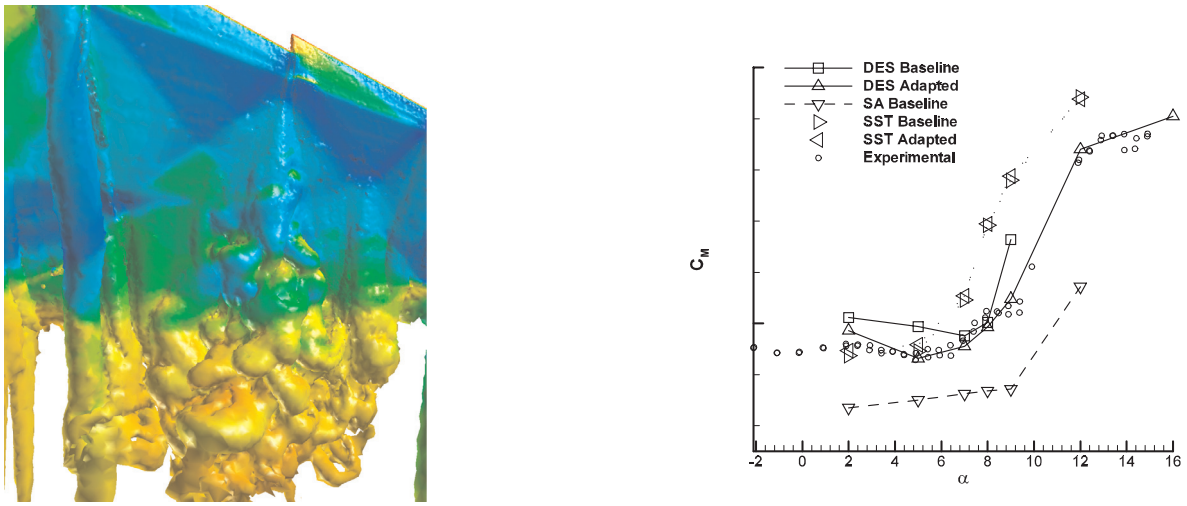
(a) (b)

Figure 2. (a) Resolved turbulent kinetic energy for various grids. (b) Power spectral density analysis of the normal force for various grids.



(a) (b)

Figure 3. (a) Flow visualisation of the vortex breakdown over the F-18A. Iso-surface of vorticity coloured by pressure. (b) Power spectral density analysis of tail pressure ports for both DES and RANS.



(a) (b)

Figure 4. (a) Flow visualisation of shock induced unsteady flow over the preproduction F/A-18E at a transonic Mach number. Iso-surface of vorticity coloured by pressure. (b) Pitching moment coefficient for DES, SA, SST and experiments.

https://doi.org/10.1017/S0001924000004656 Published online by Cambridge University Press

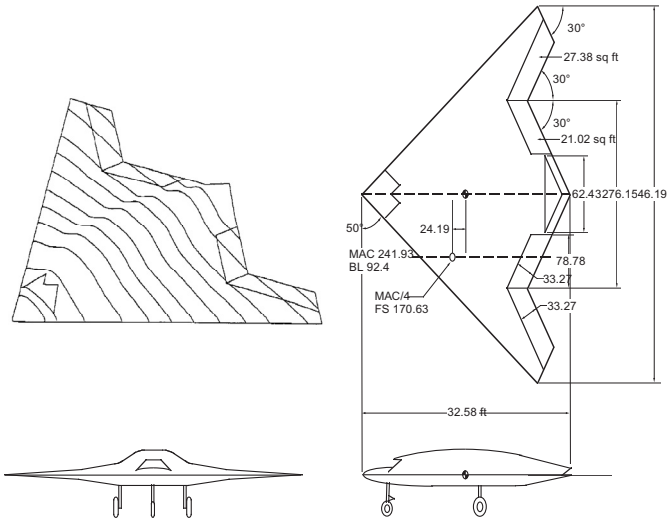


Figure 5. Boeing 1301 UCAV Configuration.



Figure 6. X-45A UCAV Configuration
(photo from NASA Dryden Flight Research Center).

second-order spatial and temporal accuracy and rigid body motion capability.

2. Use DES as the underlying turbulence treatment to obtain accurate unsteady loads and mean quantities – this requires a low dissipation solver.

3. Use adaptive-mesh refinement to improve grid resolution in critical areas with nonlinear flow field phenomena.

The proposed method requires no more additional resources than a RANS unsteady simulation for a given grid. The increase in computational time over steady-state solutions is approximately an order of magnitude due to a factor of three to make the simulation time accurate and a factor of three to acquire a sufficient number of time steps to gather statistical data. The method does require additional grid points to capture the turbulence, increasing the necessary resources.

2.6 DES results

This section presents DES results for three configurations. The first is a 70° sweep delta wing. The second and third configurations are pre-production versions of the F/A-18C and the F/A-18E.

DES combined with adaptive-mesh refinement (AMR) was used to accurately model the vortical flowfield over a slender delta wing at a Reynold's number of $1{\cdot}56 \times 10^6$ and reported by Morton *et al* [27]. The DES successfully predicted the location of the vortex breakdown phenomenon as well as the turbulent kinetic energy aft of breakdown along the vortex core. Iso-surfaces of vorticity coloured by the spanwise component of vorticity are depicted in Fig 1(a) for a $10{\cdot}5 \times 10^6$ cell solution. The solution ran 10,000 time steps requiring 10,500cpu hours on a Compaq ES45 (3·5 days on 128 processors). A coherent vortex upstream of breakdown is observed with a rapid change to chaotic turbulent flow following the breakdown point. The large number of captured scales is also evident in this figure.

Another technology that is important to the delta wing simulations is adaptive-mesh refinement (AMR). Since DES switches to LES in regions of massively-separated flow, a tool to place additional grid resolution in these separated regions is very useful.

Fig. 1(b) depicts a DES solution of an AMR grid with $3{\cdot}5 \times 10^6$ cells. The solution also ran for 10,000 time steps requiring 4375cpu hours on a Compaq ES45 (1·4 days on 128 processors). The additional scales captured for 1/3 the total number of cells of the previous grid is remarkable. Figure 2(a) shows the resolved turbulent kinetic energy along the core of the vortex for a variety of grids. As the grid is refined, the peak turbulent kinetic energy approaches the experimental value of 0·5. Figure 2(b) displays the power spectral density of the unsteady-normal force on the delta wing. Grid refinement has a dramatic effect on the resolved frequencies and shows the ability of the method to capture a range of frequencies if grid resolution is available.

After verifying that the DES method with AMR could accurately capture vortex breakdown on the delta wing, an F/A-18C was simulated using the same technique at an angle-of-attack of 30°, freestream Mach number of 0·2755, and a mean aerodynamic chord-based Reynolds number of $13{\cdot}9 \times 10^6$ (Ref. 27). The solution was computed on a grid of $6{\cdot}3 \times 10^6$ cells for 10,000 time steps and required 7,875cpu hours on a Compaq ES45 (2·6 days on 128 processors). Figure 3(a) depicts an iso-surface of vorticity coloured by pressure. The leading-edge extension vortex breakdown is evident as well as the wing leading-edge vortex. The post-breakdown windings and turbulent eddies that contribute to tail buffet are also evident. Figure 3(b) is a plot of a power spectral density analysis of an outboard-tail pressure port. Comparison of the power for the DES baseline grid solution, DES AMR grid solution, and RANS solution demonstrates the inability of RANS methods to capture the unsteadiness contributing to tail buffet. Figure 3(b) also demonstrates the improvement in the resulting power when an AMR grid is used.

DES predictions of the pre-production F/A-18E were reported by Forsythe and Woodson[28] as part of the Abrupt Wing Stall (AWS) research program. During envelope expansion flights of the F/A-18E/F in the Engineering and Manufacturing Development phase, the aircraft encountered un-commanded lateral activity, which was labeled 'wing drop.' The wing-drop events were traced to an abrupt-wing stall on either the left or right wing panel, causing a sudden and severe roll-off in the direction of the stalled wing. A production aircraft geometric modification was developed that eliminated the wing drop tendency; the modified aircraft was not simulated using DES in this study.

Wind-tunnel measurements of the pre-production F/A-18E were made by Schuster and Byrd[29], revealing highly unsteady, low frequency shock oscillations on the wing, which were identified as a potential trigger event for the 'wing drop' RANS methods were unable to reproduce these shock oscillations, even though the computations were performed in a time-accurate fashion (i.e., URANS).

Shown in Fig. 4(a) is a flow visualisation of the F/A-18E DES prediction. An isosurface of vorticity coloured by pressure is shown

https://doi.org/10.1017/S0001924000004656 Published online by Cambridge University Press

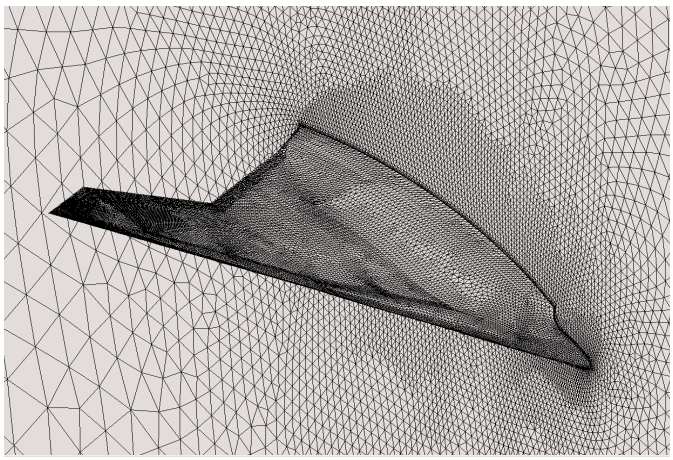


Figure 7: Unstructured UCAV Grid with 6·88 × 10^6 cells.

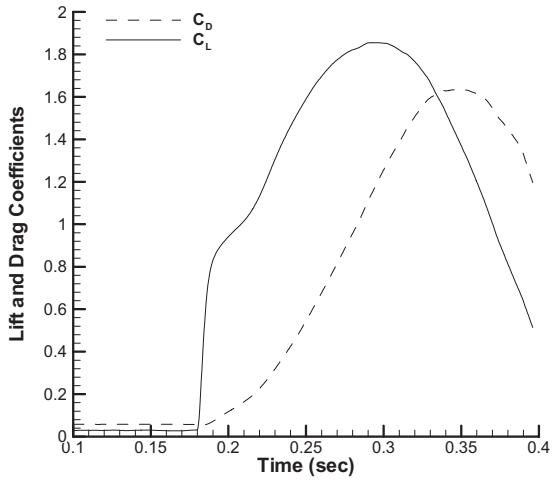


Figure 8. C_L and C_D as a function of time.

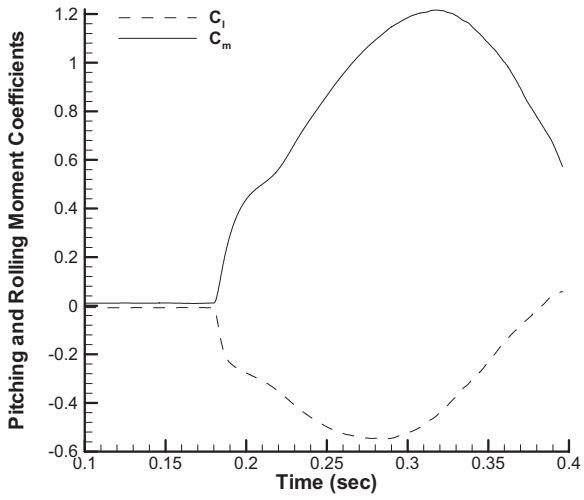


Figure 9. C_m and C_l as a function of time.

for the flow at Mach 0·9 and 9 degrees angle-of-attack. Half of the aircraft was calculated with a solution-adapted 9 × 10^6 cell grid. Solutions were run for 8,000 time steps requiring 9,000cpu hours on a Compaq ES45 (six days on 64 processors). Full aircraft calculations were also performed on meshes comprised of 18 × 10^6 cells requiring twice the number of cpu hours. Experimental measurements showed that the shock oscillated from the leading-edge flap hinge line to about mid-chord at this angle-of-attack. The DES predictions also resolved this shock motion, although with slightly less travel. In the instantaneous image shown in the figure, the shock has retreated from the flap hinge line. The separation bubble behind the shock is relatively large, and well resolved in the DES calculation, thanks to the solution-adapted grid. The minimum, maximum, and average pressures along the chord compared favorably to the unsteady experimental measurements throughout the AWS angle-of-attack range as summarised by Forsythe and Woodson[28]. The pitching moment coefficient depicted in Fig. 4(b) shows the excellent comparison of DES with an adapted-mesh solution and the experiments. It also demonstrates how far off the RANS simulations are for this case. Also note that the SST RANS results did not change on the refined grid, since the role of grid refinement in RANS is only to reduce numerical errors while fixed modeling errors remain.

To predict rigid-body motion of a UCAV the solver must also take into account the motion of the grid. Grid speed terms have been added to Cobalt and validated for various types of rigid-grid motion on simple shapes (Forsythe *et al*[30], Kotapati *et al*[31]). Rigid body motion incorporating DES has also been applied to full aircraft cases such as the F-15E spin (Forsythe *et al*[30]), F/A-18E abrupt-wing stall (Forsythe *et al*[28]), and Unmanned Combat Air Vehicle dynamic stall at low Reynolds numbers (Cummings *et al*[32]).

3.0 NOTIONAL UCAV DEMONSTRATION

A full-scale model of the Boeing 1301 UCAV configuration is shown in Fig. 5. The configuration has many similar features to the X-45A UCAV configuration (see Fig. 6). The 1301 configuration has a straight, 50° sweep leading edge, an aspect ratio of 3·1, a top-mounted engine inlet, and a B-2-like wing planform. The full-scale configuration has a mean aerodynamic chord of 20·2ft (6·2m) and a reference area of 694ft^2 (64·4m^2).

A simulation was performed for the full-scale vehicle at a freestream Mach number of 0·4, a freestream velocity of 446·7ft/s (136·2ms^{-1}), and a Reynolds number based on the mean aerodynamic chord of 57·2 × 10^6. Figure 7 shows the unstructured grid for the UCAV. The grid has 6·88 × 10^6 cells with prisms in the boundary layer and tetrahedra outside the boundary layer. The simulation consisted of 0·18 seconds (400 time steps) of flight at an angle-of-attack of 0° at the freestream conditions, followed by a simultaneous pitch and roll maneuvre for 0·22 seconds (800 time steps). A constant pitch rate of 315deg/sec was established and an initial roll rate of 0deg/sec with a roll acceleration of 1,833deg/s^2 was also performed. The simulation lasted 0·22 sec, achieving a final pitch angle of 69·3 deg and a roll angle of 44·4°. The required cpu hours for the simulation was 688cpu hours on a Compaq ES45 (on 128 processors).

Figure 8 is the time histories of the lift and drag coefficients and Fig. 9 is the pitch and roll moment coefficients as a function of time. The maximum lift coefficient achieved during the simulation is 1·855. Assuming a wing loading of 100lb/ft^2, the UCAV would have a weight of 69,400lb and the resulting maximum load for the maneuvre would be 4.4g's.

Figures 10 (a-h) depict snap-shots of the maneuvre at even increments between t = 0·18 sec and t = 0·4 sec. These visualisations show iso-surfaces of vorticity (the vorticity level was chosen to give a good representation of the separated flow) with the iso-surface being coloured by local static pressure. It is interesting to note that

https://doi.org/10.1017/S0001924000004656 Published online by Cambridge University Press

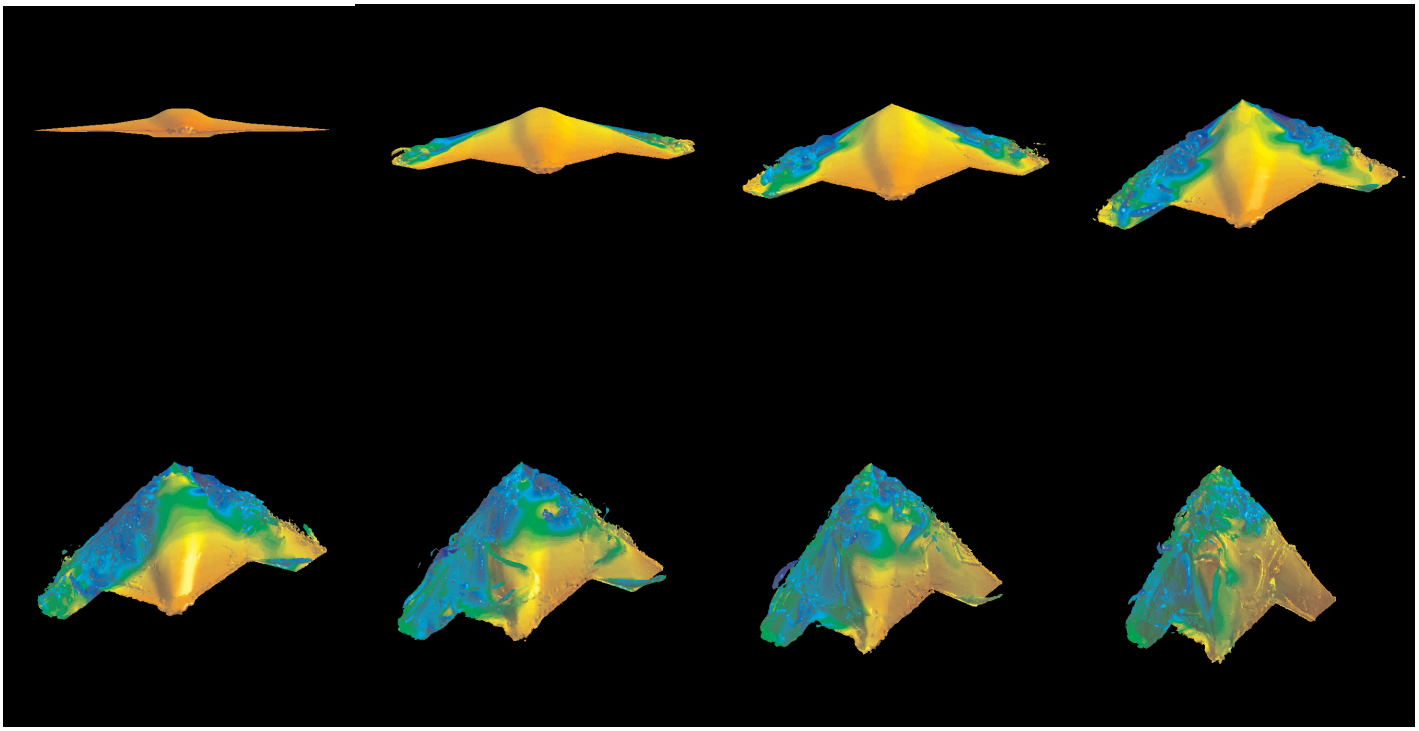


Figure 10 (a-h). Snap-shots of a pitch and roll manoeuvre. Iso-surfaces of vorticity coloured by pressure are displayed at even increments in the simulation.

although the *g* loading for the maneuvre is reasonable, the simulation displays some very complex flow field phenomena. In Fig. 10(b) vortex breakdown is observed on both the port and starboard wings and is asymmetric. The vortex breakdown proceeds upstream asymmetrically and in Fig. 10(c) fairly massive separation is observed on the port wing. Figure 10(d) shows an increase in the separated regions port and starboard as well as the interaction of an inlet vortex and the leading-edge vortex on the starboard wing. Figure 10e shows that both leading-edge vortices have broken down and the port wing is completely separated. Figure 10(f) shows interactions across the symmetry plane of the vehicle and a severely asymmetric surface pressure distribution. Figures 10(g) and *(h*) show massive separation over the entire upper surface and no coherent leading-edge vortices.

Figures 10(a-h) show the incredibly complex nature of this flow field and the high demand on the solver for accurate computation. To make this simulation completely credible, a grid sensitivity study and a time accuracy study should be performed. However, it does demonstrate the flow features necessary to be captured for an accurate simulation. This type of maneuvre would be even further complicated if an initial Mach number greater than 0·4 was used, due to shock-vortex boundary-layer interaction.

CONCLUSIONS

A method of simulating manoeuvring UCAVs has been presented. The proposed method includes an unstructured solver, Detached-Eddy Simulation, and Adaptive-Mesh Refinement. Simulations of a delta wing and two pre-production versions of the F/A-18 were presented to demonstrate the utility of the method in both the subsonic high-alpha regime and the transonic regime. Application of the method to a notional UCAV shape in a commanded pitch and roll maneuvre has also been presented. In all cases, the method has been shown to significantly improve accuracy of the simulations over traditional RANS methods for these difficult cases.

If UCAVs are going to achieve the cost savings advertised by the aerospace industry, high-resolution simulation of these difficult flight regimes must take place to reduce costly 'fixes' to the vehicles after the first test vehicle has been produced. The proposed method shows great promise in achieving, in the near term, the necessary resolution to impact the design cycle.

ACKNOWLEDGMENTS

The authors wish to thank Prof Kyle Squires of Arizona State University and Dr Philippe Spalart for their guidance and participation in the development of this method. We would also like to thank the DoD High Performance Computing Modernisation Program for the grant of computer hours, as well as, Boeing Military Aircraft in St Louis, MO for providing the UCAV 1301 geometry.

REFERENCES

1. GERN, F.H., INMAN, D.J. and KAPANIA, R.K. Computation of actuation power requirements for smart wings with morphing airfoils, April 2002, AIAA Paper 2002-1629.
2. GERN, F.H., INMAN, D.J. and KAPANIA, R.K. Structural and aeroelastic modeling of general planform UCAV wings with morphing airfoils, April 2001, AIAA Paper 2001-1369.
3. Boeing to develop UAVs with advanced propulsion, *Fuel Cells Bulletin*, November 2002, pp 4-5.
4. HUANG, A., FOLK, C., SILVA, C., CHRISTENSEN, B., CHEN, Y., HO, C.M., JIANG, F., GROSJEAN, C., TAI, Y.C., LEE, G.B., CHEN, M. and NEWBERN, S. Application of MEMS devices to delta wing aircraft: from concept development to transonic flight test, January 2001, AIAA Paper 2001-0124.
5. CAPOZZI, B.J. and VAGNERS, J. Evolving (semi)-autonomous vehicles, August 2001, AIAA Paper 2001-4241.
6. GUILMINEAU, E. and QUEUTEY, P. Numercal study of dynamic stall on several airfoil sections, *AIAA J*, 1999, **37**, (1), pp 128-130.
7. GREENBLATT, D., NEUBERGER, D. and WYGNANSKI, I. Dynamic stall control by intermittent periodic excitation, *J Aircr*, 2001, **38**, (1), pp 188-190.

https://doi.org/10.1017/S0001924000004656 Published online by Cambridge University Press

8. CARR, L.W., CHANDRASEKHARA, M.S. and WILDER, M.C. Effect of compressibility on suppression of dynamic stall using a slotted airfoil, *J Aircr*, 2001, **38**, (2), pp 296-309.
9. EKATERINARIS, J.A. and PLATZER, M.F. Computational prediction of airfoil dynamic stall, *Progress in the Aerospace Sciences*, **33**, 1997, pp 759-846.
10. CARR, L.W. Progress in Analysis and prediction of dynamic stall, *J Aircr*, 1988, **25**, (1), pp 6-17.
11. HENKNER, J. Phenomena of dynamic stall on swept wings, 22nd International Congress of the Aeronautical Sciences, August-September 2000, ICAS Paper 2000-2.9.2.
12. COTON, F.N. and GALBRAITH, R.A. An experimental study of dynamic stall on a finite wing, *Aeronaut J,* May 1999, **103**, (1023), pp 229-236.
13. MORGAN, P.E. and VISBAL, M.R. Simulation of unsteady three-dimensional separation on a pitching wing, AIAA Paper 2001-2709, June 2001.
14. SPALART, P.R. Strategies for turbulence modeling and simulation, 4th International Symposium on Engineering Turbulence Modelling and Measurements, Corsica, France, 1999.
15. SPALART, P.R. JOU W-H., STRELETS M. and ALLMARAS, S. R. *Comments on the Feasibility of LES for Wings and on a Hybrid RANS/LES Approach, Advances in DNS/LES*, 1st AFOSR Int. Conf. on DNS/LES, 4-8 August 1997, Greyden Press, Columbus, Oh, USA.
16. STRANG, W.Z., TOMARO, R.F. and GRISMER, M.J. The defining methods of cobalt: A parallel, implicit, unstructured Euler/Navier-Stokes flow solver, January 1999, AIAA Paper 99-0786.
17. SAMAREH, J. Gridtool: A surface modeling and grid generation tool, proceedings of the workshop on surface modeling, grid generation and related issues in CFD solution, 9-11 May 1995, NASA CP-3291.
18. PIRZADEH, S. Progress toward A user-oriented unstructured viscous grid generator, January 1996, AIAA Paper 96-0031.
19. SPALART, P. R. and ALLMARAS, S.R. A One equation turbulence model for aerodynamic flows, *La Recherche Aerospatiale*, 1994, **1**, p 5.
20. FORSYTHE, J.R., HOFFMANN, and K.A., DIETEKER, F.F. Detached-eddy simulation of a supersonic axisymmetric base flow with an unstructured flow solver, June 2000, AIAA Paper 2000-2410.
21. SHUR, M., SPALART, P.R., STRELETS, M. and TRAVIN, A. Detached-eddy simulation of an airfoil at high angle-of-attack, 1999, Proc 4th International Symp Eng Turb modeling and measurments.
22. SPALART, P. Young-person's guide to detached-eddy simulation grids, NASA CR 2001-211032.
23. MORTON, S.A., FORSYTHE, J.R., SQUIRES, K.D. and WURTZLER, K.E. Assessment of unstructured grids for detached-eddy simulation of high Reynolds number separated flows, 8th ISGG Conference, June 2002, Honolulu, USA.
24. FORSYTHE, J., SQUIRES, K., WURTZLER, K. and SPALART, P. Detached eddy simulation of fighter aircraft at high alpha, January 2002, AIAA Paper 2002-0591.
25. SQUIRES, K.D., FORSYTHE, J.R. and SPALART, P.R. Detached-Eddy Simulation of the Separated Flow Around a Forebody Cross-Section, Direct and Large-Eddy simulation IV, ERCOFTAC Series – Volume 8, GEURTS, B.J., FRIEDRICH, R. and METAIS, O. (Eds), Kluwer Academic Press, 2001, pp 481-500.
26. PIRZADEH, S. Vortical flow prediction using an adaptive unstructured grid method, research & technology organization applied vehicle technology panel meeting, Norway, 7-11 May 2001.
27. MORTON, S., STEENMAN, M., CUMMINGS, R. and FORSYTHE, J. DES grid resolution issues for vortical flows on a delta wing and an F/A-18C, January 2003, AIAA Paper 2003-1103.
28. FORSYTHE, J.R. and WOODSON, S.H. Unsteady CFD calculations of abrupt wing stall using detached-eddy simulation, January 2003, AIAA Paper 2003-0594.
29. SCHUSTER, D. and BYRD, J. Transonic unsteady aerodynamics of the F/A-18E at conditions promoting abrupt wing stall, January 2003, AIAA Paper 2003-0593.
30. FORSYTHE, J.R., WENTZEL, J.F., SQUIRES, K.D., WURTZLER, K.D. and SPALART, P.R. Computation of prescribed spin for a rectangular wing and for the F-15 using detached-eddy simulation, January 2003, AIAA Paper 2003-0839.
31. KOTAPATI-APPARAO, R.B., SQUIRES, K.D. and FORSYTHE, J.R. Prediction of a prolate spheroid undergoing a pitchup maneuvre, January 2003, AIAA Paper 2003-0269.
32. CUMMINGS, R., MORTON, S., SIEGEL, S. and BOSSCHER, S. Numerical prediction and wind tunnel experiments for a pitching unmanned combat air vehicle, January 2003, AIAA Paper 2003-0417.

https://doi.org/10.1017/S0001924000004656 Published online by Cambridge University Press